AAPS PharmSciTech (2024) 25:34
https://doi.org/10.1208/s12249-024-02746-5

RESEARCH ARTICLE

Novel Skin Drug Delivery Technology

Pharmacodynamic Studies of Pravastatin Sodium Nanoemulsion Loaded Transdermal Patch for Treatment of Hyperlipidemia

Seham I Elsayed[1] · **Marwa S El-Dahan**[1] · **Germeen N. S Girgis**[1]

Received: 18 July 2023 / Accepted: 16 January 2024 / Published online: 8 February 2024

Abstract

Pravastatin sodium (PVS) is a hypolipidemic drug with poor oral bioavailability due to the first-pass effect. Therefore, this study aims to formulate and evaluate transdermal patches containing PVS-loaded nanoemulsions (PVS-NEs) to increase PVS's hypolipidemic and hepatoprotective activities. PVS-NEs were prepared using the aqueous titration method, where oleic acid was chosen as an oil phase, and span 80 and tween 80 were used as surfactant and cosurfactant respectively. Droplet size (DS), polydispersity index (PDI), zeta potential (ZP), clarity, and thermodynamic stability of NEs were all characterized. Also, PVS-NEs (NE2) with 50% oil phase, 40% SC mix 2:1, and 10% water were selected as an optimum formula based on the results of DS (251 ± 16), PDI (0.4 ± 0.16), and ZP (-70 ± 10.4) to be incorporated into a transdermal patch, and PVS-NE2 loaded transdermal patches (PVS-NE2-TDPs) were prepared by solvent evaporation method. F1 patch with HPMC E15 and PVP K30 in a ratio of 3:1 represented satisfactory patch properties with good drug-excipients compatibility. Thus, it was selected as an optimum patch formula. The optimized F1 patch was characterized for thickness, moisture content, weight variation, and drug-excipients incompatibility. Therefore, it was subjected to *ex vivo* skin permeation and finally pharmacodynamic studies. *Ex vivo* permeation studies of F1 revealed that the cumulative amount of PVS permeated across rat skin was 271.66 ± 19 µg/cm^2 in 72 h, and the pharmacodynamic studies demonstrated that the F1 patch was more effective in treating hyperlipidemia than PVS-TDP (control patch) based on both blood analysis and histopathological examination.

Keywords hepatoprotective · hypolipidemic · nanoemulsion · pravastatin sodium · transdermal patches

Introduction

Hyperlipidemia is described as an abnormally high level of lipids and lipoproteins in the blood [1]. High levels of low-density lipoprotein cholesterol (LDL-C) are connected to the formation of atherosclerotic plaque [2]. The most popular lipid-lowering medications are statins, which are designed specifically to lower plasma cholesterol and lipoprotein levels by inhibiting 3- hydroxy-3-methylglutaryl coenzyme A (HMG-CoA) reductase [3]. Pravastatin sodium (PVS) is one of the statins that inhibits the previous enzyme [4]. PVS is a hydrophilic, ring-opened, dihydroxy acid with a 6\ -hydroxyl group [5]. It has been recognized that PVS has an effective antitumor activity in liver cancer and also has an effective role in wound healing [6–8]. PVS administration via the oral route has limitations, such as a short elimination half-life, considerable first-pass metabolism, and instability at stomach pH, which resulted in poor oral bioavailability (17%) [9]. Both submicron emulsion and water-in-oil nanoemulsion are colloidal dispersions that can be used to encapsulate and deliver many hydrophilic drugs [10]. Most studies have claimed that NEs are transparent, kinetically stable systems with a typical droplet size range of 10–500 nm [11, 12]. Different nanocarriers which include NEs have been used nowadays for different statins to enhance their effect [13, 14]. Formulation of NEs has several benefits, including the administration of biological and therapeutic substances. NEs help to protect drugs which are susceptible

Communicated by Nisarg Modi, Yousuf Mohammed, and Lakshmi Raghavan.

✉ Seham I Elsayed
iseham410@mans.edu.eg

[1] Department of Pharmaceutics, Faculty of Pharmacy, Mansoura University, El-Gomhoria Street, Mansoura 35516, Dakahlia, Egypt

to oxidation or hydrolysis in addition to give prolonged action of the drugs [15]. Water in oil (w/o) NEs is more effectively formulated with a mixture of surfactants than with just one, especially those of the nonionic type, such as spans and tweens. The oil phases that commonly used in NE preparation are fatty acids, such as oleic acid, esters of fatty acids and alcohols, such as isopropyl myristate, isopropyl palmitate, and ethyl oleate, medium chain triglycerides, triacetin, and terpenes, such as limonene and cineole, are all often utilized oil phase components [16]. In the present study oleic acid was selected as an oil phase in NEs preparation as it has the ability to increase the penetration through the intact skin layer [17]. Oleic acid may synergize the hypolipidemic effect of PVS and reduce the risk of cardiovascular diseases [18]. In transdermal drug delivery systems (TDDs), micro emulsion (ME) and NEs formulations are promising strategies [15]. Since the dermis has a rich blood supply that makes it easier for the drug to enter systemic circulation directly, TDDs are intensively researched as a smart route for drug administration [19, 20]. Based on what was mentioned above, this study's purpose was to formulate PVS-NEs-TDPs as an alternative to the oral route to avoid its disadvantages. Physicochemical characteristics, *in vitro* and *ex vivo* drug release will be evaluated. Finally, the pharmacodynamic activity of the optimum patch formula (F1) will be assessed on hyperlipidemic-induced animals.

Materials and Methods

Materials

Pravastatin sodium (PVS) was supplied by Delta Pharm Pharmaceutical Co., Cairo, Egypt**.** Oleic acid was purchased from LANXESS, Energizing Chemistry, Cologne, Germany. Sorbitan Mono Oleate (Span 80) was purchased from Oxford Laboratory Chemicals. Polyoxyethylene 20 sorbitan monooleate (Tween 80) and Polyethylene glycol 400 (PEG) were obtained from Adwic—El-Nasr Pharmaceutical Chemicals, Qaliubiya, Egypt. Hydroxypropyl methylcellulose E15 (HPMC, 15MPa.s) and Polyvinylpyrrolidone (PVP) with a molecular weight 44.000 Da (PVP K30) were supplied by Eipico pharmaceutical company, Egypt. Eudragit RS100 and Eudragit RL100 were obtained from Evonik Pharmaceutical Company, Germany. Poloxamer 407 was purchased from BASF SE, Germany. HPLC grade methanol, Dimethyl sulfoxide (DMSO), and dichloromethane were obtained from Fischer Scientific UK. Diamond Diagnostics, Holliston MA, USA provided the kits for the examination of albumin and liver enzymes. Lipid profile assay kits were obtained from Spinreact company in Spain.

Preparation of Nanoemulsion (NEs)

Selection of Oils, Surfactants, and Cosurfactant

Different oils (Oleic acid, Caster, Soybean, Capryol 90, and Maisine), as well as various surfactants and cosurfactants (Span 80, Tween 80, and Labrafile ML 1944), were used to measure the PVS saturation solubility [21]. An excess amount of PVS (50 mg) was added to 2 ml of the solvent and shaken continuously for 72 h at 25 ± 1°C in separate stoppered vials to get equilibrium using a thermostatically controlled agitating water bath (Grant Instrument, Cambridge Ltd., UK). After that, the vials were taken out and centrifuged for 20 min at 5000 rpm. The supernatant was filtered using a membrane filter (0.45µm). Solubility was determined by UV spectrophotometer (SpectroUV-VIS double beam, Labomed Inc.USA) at λ_{max} 238 nm after appropriate dilution with methanol. The oil, surfactant, and co-surfactant in which PVS was highly soluble were selected for further study.

Construction of Phase Diagram

For the creation of pseudo-ternary systems, oleic acid, span 80, and tween 80 was chosen as a surfactant, and cosurfactant oil phase respectively based on the results of solubility studies. Accordingly, three combinations of the two substances were created (1:1, 2:1, and 3:1 v/v) by combining different ratios of the surfactant (span 80) and cosurfactant (tween 80). The three surfactant co-surfactant mixtures (SC mix) were evaluated visually for clarity, miscibility, and ease of flow. To prepare the SC mix they were mixed at the desired ratio and allowed to equilibrate overnight as previously reported [22]. A precise amount of oil and SC mix were mixed at room temperature using a magnetic stirrer at 800 rpm (Magnetic stirrers, Thermolyne Corporation, Dubuque Iowa, USA), then water was added dropwise (50 µl per 5 min), and the mixture was visually examined for clarity and transparency after 24 h. Titration with the aqueous phase was continuous until the mixture became turbid. The oil and SC mix were mixed in ratios of 1:9, 2:8, 3:7, 4:6, 5:5, 6:4, 7:3, 8:2 and 9:1 respectively. NE zone was drawn for each phase diagram, and the larger the area, the more effective the self-nanoemulsification [23].

Preparation of PVS-NEs

Three formulations of PVS- NEs (NE1, NE2, and NE3) were formulated using 50% v/v of oleic acid, 40% v/v of SC and 10% v/v of water. Initially, both the SC mix and the oil phase were mixed using a magnetic stirrer at 600 rpm for 5 min. After that, PVS was dissolved at a consistent concentration (10 mg/0.2 ml) in the aqueous phase and then added gradually

to the previous mixture to prepare PVS-NEs using the aqueous titration method [24]. Further mixing of the formed NEs was made by an ultrasonic homogenizer at 60% amplitude for 2 min in an ice bath (Ultrasonic homogenizer, 4710 Series, Cole-Parmer Instrument Co., Chicago, USA) [25].

Characterization of PVS–NEs

Accelerated Physical Stability Tests

The physical stability of NEs was evaluated using the techniques described by Kaur, R., and M. Ajitha [26], where NEs were centrifuged for 30 min at 5000 rpm. After that, the formulations were subjected to six heating and cooling cycles between an oven and a refrigerator, with 48 h of storage at each temperature. (The oven is Gering type SPA-GELMAN, Germany). Since no phase separation was observed, we tested the stable formulations using a freeze–thaw cycle, where for each formulation, three freeze–thaw cycles between -20°C and 25°C were performed. The formulation's creaming, phase separation, coalescence, and cracking were all evaluated. For further investigation, the formulation that passed thermodynamic stability tests was selected for further study.

Determination of Droplet Size (DS), Polydispersity Index (PDI), and Zeta Potential (ZP)

The DS, PDI, and ZP of NEs droplets were measured by photon correlation spectroscopy (Malvern Instruments Ltd., Malvern, Worcestershire, UK). The Samples then were measured after being diluted with filtered refined oleic acid at a ratio of 1:50 (v/v) and equilibrated for 2 min inside the instrument before measurement to prevent multiple scattering effects as previously reported by Polychniatou, V. and C. Tzia [27]. Each sample was measured in triplicate and data were provided as mean ± S.D.

Drug Content

The prepared NEs were dissolved in methanol and then analyzed spectrophotometrically against the blank solution of NE [15].

Transmission Electron Microscopy (TEM)

The morphology of the optimum NEs (NE2) was checked by Transmission electron microscope (JEOL JEM -2100, JEOL Ltd, Tokyo, Japan) after proper dilution with filtered refined oleic acid [28].

In Vitro Release Studies of PVS from NE2

NE2 was selected as an optimum NE formula according to DS, PDI, ZP, and drug content. The release of PVS from NE2 was performed using modified Franz diffusion cells continuously stirred at 100 rpm at 37°C during the entire experiment in a GFL shaking, incubator (Gesellschaft fur Labortechnik Burgwedel, Germany). The synthetic cellophane membrane that separated the donor and receptor compartments had a molecular weight cutoff of 12,000–14000 Dalton. Therefore, two ml of NE2 was placed over the membrane and 100 ml of phosphate buffer PBS (pH 7. 4) was added to the receptor, three ml samples were taken out and replaced with an equal volume of fresh buffer at time intervals of 0.5, 1, 2, 3, 4, 5, 6, 7, 8, 24, 48 and 72 h. The withdrawn samples were suitably diluted and analyzed spectrophotometrically at 238 nm to determine % drug released [29].

Stability Studies of NE2

Stability studies of the optimized NE2 were conducted by storing the samples for 3 months at refrigerator temperature 4 ± 2°C, at room temperature 25 ± 2°C, and oven temperature 40 ± 2°C. After that, the formulation samples were evaluated for their, DS, PDI, ZP, and drug content at 0, 1, 2, and 3 months [30]. All tests were done in triplicates.

Preparation of Transdermal Patches (TDPs)

NE2 was selected as an optimum NE formula to be incorporated into the transdermal patch according to DS, PDI, ZP, and drug content. Then PVS-NE2-TDPs were prepared by solvent evaporation method [31]. Compositions of different formulations are shown in Table I. The selected polymers at different ratios were precisely weighted and dissolved in 8 ml of dichloromethane and methanol by a ratio of (4:1) using a magnetic stirrer at 100 rpm for 20 min to form a clear solution. Then PEG 400 and DMSO were added as a plasticizer and penetration enhancers respectively to 8 ml of the optimum PVS-NE2 containing 40 mg of PVS then added dropwise to the above clear solution stirred at 100 rpm for 1 h to evaporate the organic solvent. The resulting uniform solution was cast into a glass plate with a diameter of 7 cm and a total area of 38.5 cm^2 then dried at room temperature for 48 h and under vacuum for 2 h. The dried patches were cut, encased in aluminum foil, and kept in a desiccator for the next studies. A control patch (Fc) was prepared with the same procedure using PVS alone.

Physicochemical Evaluation of PVS-NEs-TDPs

Physical Examination

All transdermal patches were visually examined for their smoothness, clarity, color, flexibility, and homogeneity.

Table I Composition of PVS-NE2-TDPs

Formulation	Volume of NE2 or the equivalent amount of PVS (mg)[a]	HPMC E15 (mg)[b]	PVP K30 (mg)[c]	ERS100 (mg)[d]	ERL100 (mg)[e]	PEG400 (mg)[f]	DMSO (mg)[g]
F1	8 ml of NE2	300	100	-	-	120	30
F2	8 ml of NE2	300	-	100		120	30
F3	8 ml of NE2	350	50			120	30
F4	8 ml of NE2	350		50		120	30
F5	8 ml of NE2	300			100	120	30
F6	8 ml of NE2	350			50	120	30
Control patch (Fc)	40 mg PVS	300	100	-	-	120	30

[a]PVS; pravastatin sodium

[b]HPMC; hydroxy propyl methylcellulose E15

[c]PVP K30; Polyvinylpyrrolidone K30

[d]ERS100; Eudragit RS100

[e]ERL100; Eudragit RL100

[f]PEG; polyethylene glycol

[g]DMSO; dimethylsulphoxide

Thickness

The thickness of the whole medicated patches was measured at five different positions using a micrometer screw gauge (Mitutoyo, Japan) [32]. The results were expressed as mean ± SD.

Folding Endurance

The test was manually conducted on three different patches (1 cm^2 each) and the folding endurance value was calculated by counting how many times the patch could be folded at the same place without tearing or breaking [33]. The results were then expressed as mean ± SD.

Weight Variation

Variation in the weight of medicated patches was calculated by weighing six individual ones (1cm^2 each) using Electric Balance (Zakiady Mechanikr Precyzyjnej Merrwag Gdansk, Poland). The mean and SD were then calculated [34].

Drug Content Uniformity

Patches (1 cm^2 each containing 1mg of PVS) were dissolved in a measuring flask containing 100 ml methanol, and the content was magnetically stirred for 2 h. The solution was then filtered and diluted with methanol and then analyzed spectrophotometrically against a blank solution of plain [35], and the results were expressed as mean ± SD.

Mechanical Properties of F1 Patch

The tensile strength, percent elongation at break, and modulus of elasticity (Young's modulus) of both medicated and plain patches were measured using Universal Testing Machine (UTM) (Model LRX-plus LIoyd Instruments Ltd. Fareham, UK). This machine's sensitivity ranges from 0 to 5,000 N. (500 kg), and there are two loaded cell grips in it, a bottom fixed cell grip and a top moveable one. These cell grips were positioned at intervals of 4 cm to approximate the patch length, and strips of the patch with dimensions of 4 cm length and 2 cm width were cut and fixed between them, and the measurements were made at a speed of 50 mm/min. The load placed on the patch was then automatically raised at a set rate until the patch broke, and the mechanical characteristics of the F1 patch were estimated using the following equations [36].

$$\text{Tensile strength (B)} = F/A \quad (1)$$

where F is the maximum force required to break the patch and A is the cross-sectional area of the patch.

The percentage elongation of patches was calculated using Eq. 2, where Lf is the patch length before breaking, while Li is the patch's original length:

$$\%\ \text{Elongation} = (Lf - Li)/Li \times 100 \quad (2)$$

Young's modulus (ME) is calculated according to Eq. 3, Where B is tensile strength and ME is Young's modulus:

$$B = ME\frac{Lf - L0}{L0} \quad (3)$$

Determination of Moisture Content

All patches were accurately weighed at zero time (initial weight) and then kept in a desiccator containing anhydrous calcium chloride after 3 days they were weighed again (final weight) and % moisture content was calculated based on Eq. 4 [37].

$$\%\ \text{Moisture content} = \frac{(\text{Initial Weight} - \text{Final weight}) \times 100}{\text{Initial weight}} \quad (4)$$

Drug Excipients Incompatibility

Fourier-Transform Infrared spectroscopy (FT-IR)

FT-IR was used to investigate drug excipients incompatibility between the component of both the optimum NE2 and the optimum patch (F1) using FTIR spectrophotometer (Nicolet iS10, Thermo Fisher Scientific, USA), where the scanning range was from 500 to 4000 cm^{-1} [38].

In Vitro Release Studies of PVS from PVS-NEs-TDPs

The *in vitro* release of PVS from the prepared PVS-NE2-TDPs was conducted using modified Franz cells stirred at 100 rpm at 37°C during the entire experiment in GFL shaking incubator. Then, patches (1 cm^2 each) containing 1 mg of PVS were placed over the membrane and the receptor was filled with 20 ml PBS (pH 7.4). After that, 3 ml samples were taken out from each cell and replaced with an equal volume of fresh buffer at time intervals of 0.5, 1, 2, 3, 4, 5, 6, 7, 8, 24, 48, and 72 h suitably diluted and analyzed spectrophotometrically at 238 nm to determine % drug released using a blank of plains [39]. Each experiment was conducted in triplicate and SD was calculated.

Ex Vivo Permeation Experiment

Skin Preparation

The rat dorsal skins were shaved, and the subcutaneous fat was removed, and its integrity was examined before washing to exclude the damaged parts. Then the freshly excised skin was soaked in PBS (pH7.4) containing 0.02% sodium azide as a preservative and kept in the refrigerator (4 ± 2°C) overnight just before performing the experiment [40].

Ex Vivo Permeation Study

The skin samples were wisely tied to modified Franz diffusion cells each of 1 cm^2 diffusion area, so that the stratum corneum facing the donor compartment while the receptor compartment was filled with 20 ml PBS (pH 7.4) containing 0.02% sodium azide the sets were stirred at 100 rpm at 37 ± 0.5°C during the experiment. The prepared patches each of 1cm^2 and containing 1 mg of PVS were applied over the membrane in the donor compartment. At predetermined time intervals of 0.5, 1,2, 3, 4, 5, 6, 7, 8, 24, 48, and 72 h, 3 ml were taken out from the release media and replaced immediately with the same volume of fresh buffer. The samples were diluted and analyzed spectrophotometrically at 238 nm to determine % drug released using blank of plains as previously reported [33]. Each experiment was done in triplicate and SD was calculated [35].

Kinetics Studies

The release profiles of PVS were analyzed according to mathematical models, zero-order kinetics [41], first-order kinetics [42], Higuchi equation [43], and Korsmeyer Peppas equation to determine the release model that describes PVS release patterns [44].

Stability Studies of the Optimized F1 Patches

Stability studies of the optimum patch (F1) were conducted for 6 months at ambient temperature (25 ± 2°C) and refrigerator temperature (4 ± 1°C). All patches were encased in aluminum foil during the study and examined every two months regarding their physical appearance, *in vitro* drug release as well as drug content [45].

In Vivo Studies

The Faculty of Pharmacy Ethics Council for the Care and Usage of Laboratory Animals at Mansoura University in Egypt accepted the animal protocol code number (82–2023). Sprague–Dawley healthy rats (weighing 250–300 gm) were given a week to acclimatize to the experimental conditions, such as humidity and temperature, and were fed a standard rat pellet diet. The animals were kept at room temperature with unrestricted access to water during the experiment.

Skin Irritation Test

Skin irritation was performed on six healthy rats (weighing 250–300 mg). Where the dorsal surface of rats was shaved and cleaned well with rectified spirit. F1 patch (3 cm^2 each) was then put on the dorsal surface [46]. The transdermal patches were removed after 24, 48, and 72 h, and the skin was examined for edema and erythema. Finally, the rats were euthanized, and the tested skin areas were separated for histologic examination using a light microscope (Olympus Tokyo Japan) [47].

Pharmacodynamic Studies

Pharmacodynamic studies were conducted to compare the hypolipidemic activities of the F1 patch to those of PVS-TDP (control patch) and PVS solution according to our previously published research [48]. In this study, thirty healthy male rats were divided into five groups with six rats in each group.

G1 served as the negative control.
G2 served as the positive control (injected with poloxamer 407 only).
G3 was hyperlipidemic rats treated with free PVS solution orally (10 mg /kg /day) [46].
G4 was hyperlipidemic rats treated transdermally by a control patch (Fc) with an area of 3 $cm.^2$. (Contains 3 mg of PVS)
G5 was hyperlipidemic rats treated transdermally by PVS- NE2 – TDP (F1 patch) with an area of 3 cm^2.

Induction of Hyperlipidemia

Before the experiment, rats were fasted overnight with unrestricted access to water. Then, the lipid profiles were assessed to rule out rats with hyperlipidemia. Poloxamer 407 solution (1 g/Kg) was administered intraperitoneally in a single dose to induce hyperlipidemia [49, 50]. The experimental rats' hyperlipidemia was confirmed after 12 h of poloxamer 407 administration. As a result, the rats received numerous doses of free PVS solution (10 mg/kg/day) orally for one week, as well as the equivalent of Fc patch and F1 patch transdermally [46]. Blood samples were withdrawn 3, 4, 5 days, and 1- week after the initiation of treatment to analyze specific biomarkers.

Collection of Blood and Tissue Samples

Using non-heparinized microhematocrit capillary tubes, blood samples were taken from each rat's retro-orbital vein throughout the treatment period while they were under the anesthesia of ketamine (12 mg/kg) and xylazine (1 mg/kg) [51, 52]. After coagulation of blood samples, serum was collected using cooling centrifugation at 3000 rpm for 20 min. The serum was then stored at -20°C until the *in vitro* diagnostic kits' assay was done.

Histopathological Examination

Rats were euthanized and immediately laparotomized, and their livers and quadriceps muscles were collected, prepared, and saved for histological examination in 10% buffered formalin [53]. Hematoxylin and eosin (H and E) were used to visualize sections of the liver and quadriceps muscles under a light microscope after they had been fixed on slides, deparaffinized, and stained [54].

Statistical Analysis

One-way ANOVA followed by Tukey–Kramer multiple comparisons and Student's *t*-test (un-paired) were performed for *in vitro* and *in vivo* data respectively using Graph Pad Prism software version 8 (Graph Pad Software, San Diego, CA, USA). $P < 0.05$ was considered a significant. The results were presented as mean ± SD for *in vitro* and mean ± SEM for *in vivo* data.

Results and Discussion

Selection of Oils, Surfactants, and Cosurfactants

The solubility results of PVS in oils, surfactants, and cosurfactants showed that oleic acid (26 ± 4) mg/ml, span 80 (16 ± 2) mg/ml, and tween 80 (21.5 ± 1) mg /ml achieved the highest solubility of PVS. Therefore, oleic acid, span 80 and tween 80 were chosen as the oil phase, surfactant, and cosurfactant for NEs preparation respectively.

Construction of Phase Diagram

The three SC mix combinations (span 80: tween 80) (1:1, 2:1, and 3:1v/v) were used to prepare pseudo-ternary systems of oleic acid, SC mix combination, and water as illustrated in Fig. 1. A concentration of 50% v/v of oleic acid, 40% v/v of SC mix combination, and 10% w/w of water were chosen from the NEs area of the pseudo-ternary diagrams to prepare w /o NE of PVS. These components are recognized as safe excipients to the skin as issued by the FDA [55].

Preparation of PVS–NEs

Three formulations of PVS- NEs (NE1, NE2 and NE3) were prepared as illustrated in Table II.

Characterization of the Prepared PVS-NEs

Accelerated Physical Stability Tests of NEs

PVS-NEs systems exhibited physical stability during heating, cooling, freeze–thaw cycles, and centrifugation cycles as they showed no drug precipitation or phase separation.

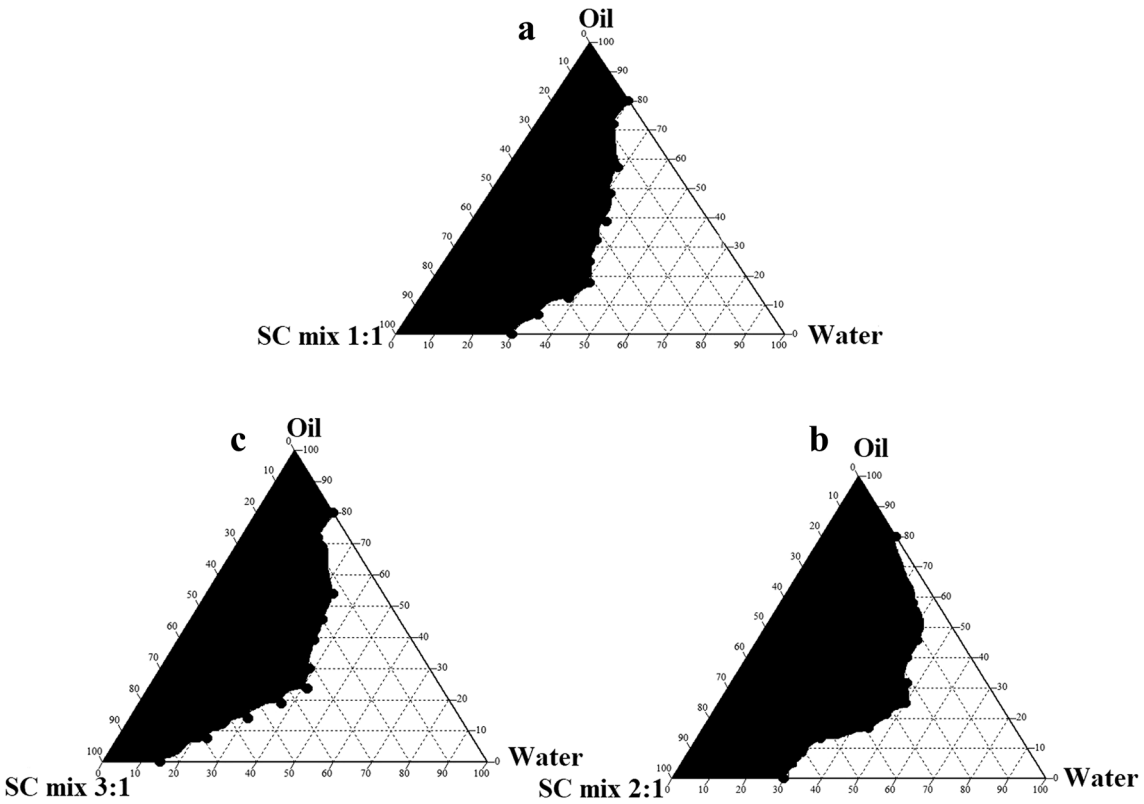

Fig. 1 Pseudo-ternary phase diagrams for drug-free nanoemulsion with SC mix values of **a** 1:1, **b** 2:1, and **c** 3:1

Analysis of DS, PDI, and ZP

The average DS of the prepared NEs ranged from 251 ± 16 to 385 ± 20 nm, while the PDI ranged from 0.38 ± 0.1 to 0.45 ± 0.1 and ZP values ranged from -20 ± 3.6 to -70 ± 10.4 mv as shown in Table II. The droplet size appeared to be high in all formulations. This may be due to the higher solubility of PVS in oleic acid which increases the PVS amount in the oil phase and thus increases the size of the droplet. A similar finding was previously reported [56, 57]. Also, the angular structure of oleic acid could cause larger particles [58].

Drug Content

The drug content of PVS-NEs ranged from 95 ± 2.5 to 100 ± 3.8 as shown in Table II which indicated good drug loading capacity of NEs.

Selection of the Optimized NEs Formula

NE2 was selected as an optimum PVS-NEs formula as it showed the smallest PS (251 ± 16) nm with narrow size

Table II The Average Droplet Size, PDI, ZP, and Drug Content of PVS-NE2

Code	SC Mix ratio (Span 80: Tween 80)	Oleic acid %	SC Mix [a] ratio %	Water%	Average droplet size (nm)	PDI [b]	ZP (mv) [c]	Drug content%
NE1	1:1	50	40	10	310 ± 65	0.38 ± 0.1	-69 ± 20	95 ± 2.5
NE2	2:1	50	40	10	251 ± 16	0.4 ± .16	-70 ± 10.4	100 ± 3.8
NE3	3:1	50	40	10	385 ± 20	0.45 ± .1	-20 ± 3.6	97 ± 2.5

Data are represented as mean ± SD ($n = 3$)

All system contained 50% oleic acid, 40% SC mix, and 10% distilled water

[a]SC mix; surfactant co-surfactant mixture

[b]PDI; polydispersity index

[c]ZP; zeta potential

distribution PDI (0.4 ± 0.16), the highest ZP (-70 ± 10.4) mv and the highest drug content (100 ± 3.8) %. So NE2 was selected for further evaluation to be incorporated into TDPs.

Transmission Electron Microscopy (TEM)

The optimum NE2 morphology was examined using TEM as shown in Fig. 2 which revealed that NE2 droplets were spherical, dark, and well dispersed similar results were previously reported [59, 60].

Stability Studies of NE2

During stability studies, DS, PDI, ZP, and drug content were evaluated at 0, 1, 2, and 3 months in three different temperatures (Table III). It was found that the optimized NE2 showed no drug precipitation or phase separation in different temperatures. There was no significant change ($p > 0.05$) in DS, PDI, ZP, or drug contents throughout the storage period at refrigerator temperature (4 ± 2°C). However, at room temperature (25 ± 2°C), there was a significant decrease in DS in the third month and a significant decrease in ZP starting from the second month. Also, In the oven temperature (40 ± 2°C), a significant reduction in DS from the second month and a decrease in ZP from the first month were observed. The decrease in DS may be due to the nature of PVS which must be stored at a lower temperature [9, 61] and the oil droplets that have been fully solubilized in tween 80 micelles for an extended period [56, 62, 63]. This indicated that lower temperature had a better effect on NE2 stability [25, 57].

Preparation of Transdermal Patches

All patches were prepared by a solvent evaporation method using dichloromethane and methanol by a ratio of (4:1) as a solvent for different polymers. The composition of different patches is overviewed in Table I.

Physicochemical Evaluation of the PVS-NEs-TDPs

Visual examination of the prepared patches demonstrated their smoothness, clarity, flexibility, and homogeneity. Also, the measured thickness ranged from 0.817 ± 0.1mm to 0.89 ± 0.5 mm, the measured weight ranged from 130 ± 7mg to 146 ± 6 mg, the measured drug content ranged from 90 ± 8% to 98.66 ± 4.5%, and the measured moisture content ranged from 10 ± 3% to 11.8 ± 3%. The Physicochemical properties of the prepared patches are presented in Table IV.

Based on physicochemical properties F1 patch which was prepared using HPMC E15 and PVP K30 in a ratio of 3:1 achieved satisfactory physicochemical properties, so it was selected as an optimum patch formula for further evaluation and permeation study.

Mechanical Properties of F1 Patch

F1 patch showed satisfactory tensile strength, % elongation 25 ± 2.5%, and modulus of elasticity 0.727 ± 0.041 (Kg/cm^2). This indicated that F1 patch would preserve its integrity during application on the skin.

The Fourier Transform Infrared Spectroscopy (FT-IR)

Figure 3 depicts FT-IR spectra of the optimized NE2 formula (Fig. 3a) and the optimized F1 patch formula (Fig. 3b). The distinctive absorption peaks of PVS (Fig. 3I) show peaks corresponding to hydroxyl bond stretching (O–H) at 3419 cm^{-1}, carboxyl bonds stretching (C = O) at 1727 cm^{-1} and alkenes stretching (C = C) at 1569 cm^{-1} which are distinctive peaks of PVS as previously reported by [9, 64, 65]. The spectrum of oleic acid (Fig. 3a. II) shows two sharp peaks at 2923 and 2856 cm^{-1} which is attributable to stretching vibrations of the C-H atom, sharp bands at 1710 cm^{-1} owing to stretching vibration of C = O, and a sharp peak at 1287 cm^{-1} owing to C-O stretching vibration [66]. Besides,

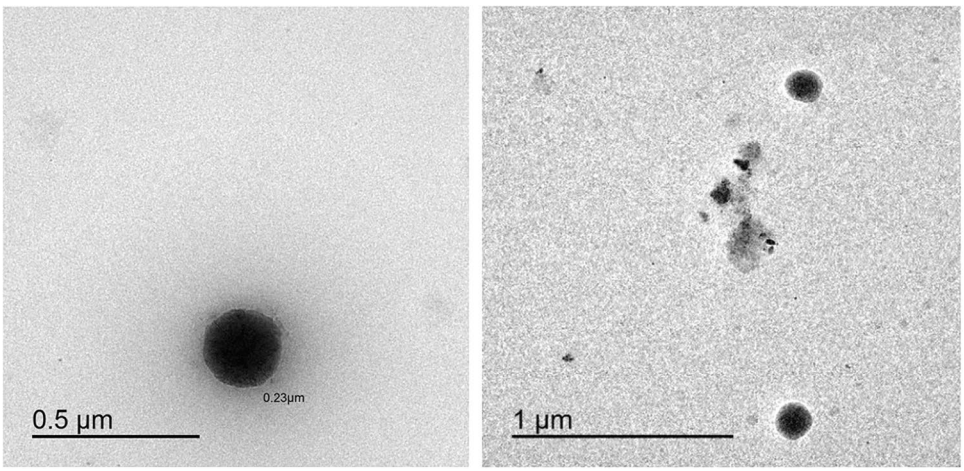

Fig. 2 Transmission electronic microscopy image of the optimized PVS-NEs formula (NE2)

Table III Storage Stability Data of NE2 at Different Temperatures

Temperature (°C)	Time	Droplet size (nm)	PDI [a]	ZP (mv) [b]	Drug content (%)
4 ± 2°C	zero	253 ± 20	0.4 ± .11	-83 ± 11	100 ± 3
	First month	230 ± 22	0.64 ± 0.15	-72.9 ± 7	99 ± 2
	Second month	272 ± 12	0.6 ± 0.15	-69.66 ± 4.5	98 ± 1
	Third month	230 ± 19	0. 61 ± 0.046	-68 ± 2.6	95 ± 1
25 ± 2°C	Zero	253 ± 20	0.4 ± 0.16	-83 ± 11	100 ± 2
	First month	220.3 ± 10	0.427 ± 0.18	-66 ± 10	96 ± 3
	Second month	237.3 ± 25.5	0.2 ± .15*	-55.1 ± 7.2*	90 ± 2
	Third month	126.33 ± 32*	0.212 ± 0.1*	-54 ± 5.3*	90 ± 1
40 ± 2°C	Zero	253 ± 20	0.4 ± 0.16	-83 ± 11	99 ± 1
	First month	222 ± 10	0.09 ± 0.05*	+ 60.3 ± 9*	90 ± 1
	Second month	134 ± 14*	0.08 ± 0.05*	+ 57 ± 8.7*	88 ± 8.88
	Third month	144 ± 61*	0.44 ± 0.3	+ 59 ± 4*	80.6 ± 1.5*

Each value denotes the mean ± SD. The statistical analysis was performed at $p < 0.05$. *Indicates a significant difference vs initial

[a]PDI, poly dispersity index

[b]ZP, zeta potential

the spectrum of span 80 (Fig. 3a.III) shows a wide peak at 3420 cm^{-1} owing to O–H stretching, at 2855 cm^{-1} corresponding to C-H stretching, at 1741 cm^{-1} owing to stretching of C = O, at 1464, and 1378 cm^{-1} owing to bending of C-H [67]. Whereas the spectrum of Tween 80 (Fig. 3a. IV) shows distinctive peaks at 3448 cm^{-1} owing to O–H stretching, at 2870 cm^{-1} owing to stretching of C-H, at 1738 cm^{-1} that is attributable to C = O stretching vibration [67].

PVS distinctive peaks disappeared in the spectrum of the medicated NE2 (Fig. 3a.VI) which confirms the encapsulation of PVS into NEs droplets and the FTIR spectra of PVS, HPMC E15, PVP K30, the physical mixture of F1, the plain, and the medicated patches of F1 are illustrated in Fig. 3b.

HPMC spectrum (Fig. 3b.II) exhibits stretching peaks in the area 3481 cm^{-1} that is assigned to stretching frequency of O–H, at 2933 cm^{-1} for stretching vibration of C-H, at 1654 cm^{-1} for stretching of C = C in aromatic ring, and at 1379 cm^{-1} is due to bending vibration of hydroxyl group as previously reported by [68].

The IR spectrum of PVP K30 (Fig. 3b.III) shows the distinctive peaks observed at 3455 cm^{-1} which is attributable to the stretching of O–H and at 1660 cm^{-1} owing to the stretching of C = O bending [69, 70]. While the distinctive absorption band of PVS still appeared in the FTIR spectrum of the physical mixture (Fig. 3b.IV).

As for plain and medicated patches, their FTIR spectrum shows a broad band at 3000–3600 cm^{-1} of free O–H hydroxyl group and intermolecular/intramolecular hydrogen bonding between components of the patches.

In Vitro PVS Release from the Optimized NE2 and the Optimized F1 Patch

The % release from the PVS solution was 33.6 ± 3.5% in the first 0.5 h and 100% after 4 h Fig. 4a. Whereas, the PVS % released was 20.66 ± 1.15% and 18 ± 2% in 8 h which was an initial burst release from the optimized PVS-NE2 and the optimized F1 patch respectively followed by a sustained release for 72 h [71]. Also, the % release of PVS was 63 ± 2.6% and 51.6 ± 2.9% from the NE2 and F1 patch respectively throughout 72 h as shown in (Fig. 4a). The burst release of PVS due to the eroded outer layer of NE2 and the sustained release may be due to PVS being

Table IV Results of Physicochemical Parameters

Patch code	Thickness (mm)	Folding endurance	Weight variation (mg)	Drug content (%)	Moisture content (%) (fold)
F1	0.817 ± 0.1	270 ± 10	146 ± 6	98.66 ± 4.5	11.8 ± 3
F2	0.85 ± 0.2	220 ± 20	144 ± 9	90 ± 8	10 ± 2
F3	0.89 ± 0.5	260 ± 10	140 ± 4	95.7 ± 4.5	11.4 ± 3
F4	0.82 ± 0.3	215 ± 30	130 ± 7	95 ± 7	11 ± 2
F5	0.86 ± 0.4	230 ± 20	143 ± 8	93 ± 7	10 ± 1
F6	0.85 ± 0.3	235 ± 40	142 ± 6	96 ± 8	11 ± 2

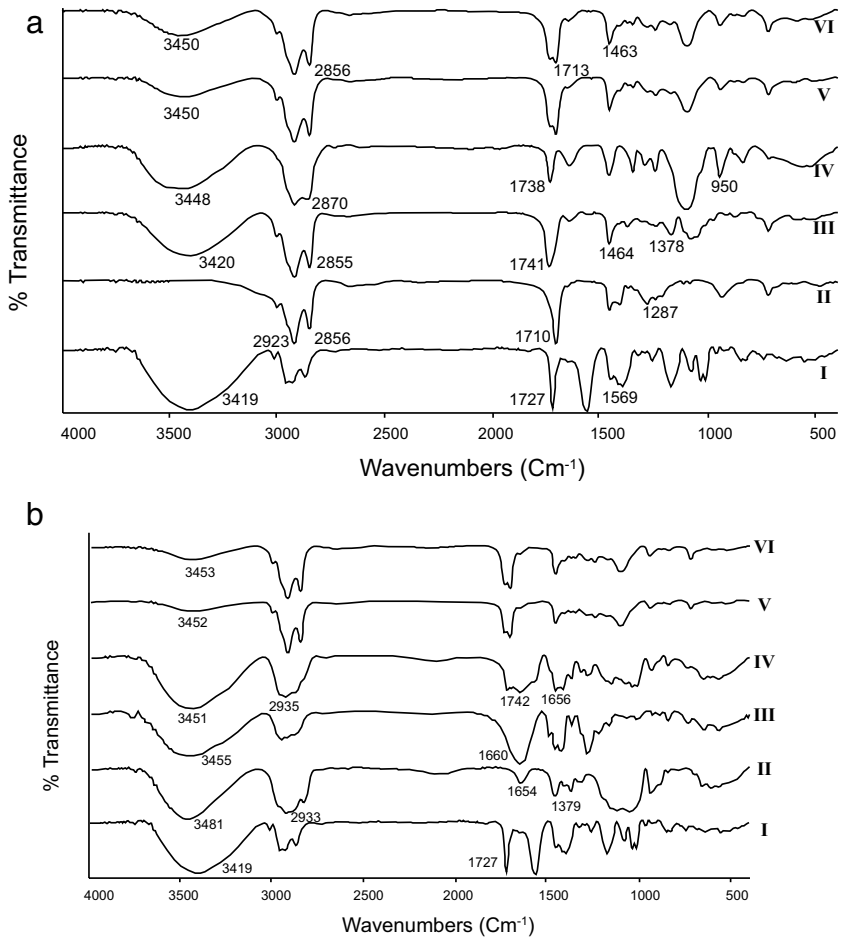

Fig. 3 Fourier Transform Infrared Spectroscopy (FT-IR)

entrapped in the core of NE2 and the oily phase acting as a barrier for the hydrophilic drug transport [72, 73].

F1 was selected as an optimum patch formula for incorporation of PVS-NE2 based on % PVS release from each formula of the prepared TDPs. Figure 4B depicts the % release of PVS from the different patches that could be arranged as follows: F1 > F3 > F6 > F5 > F4 > F2. The % release of the prepared six patches was 61 ± 2.6%, 48 ± 2.7%, 45.3 ± 1.5%, 43.7 ± 2%, 41 ± 1% and 36 ± 1 respectively. From these results, we can observe that the % release was found to be higher for F1 and F3 patches compared to other patches because they had a higher portion of hydrophilic polymers (HPMC E15 and PVP K30) as compared to other formulations. This may be due to the dissolution of an aqueous soluble fraction of the polymer matrix leading to minute pores formation [74, 75]. The same results with hydrophilic polymers were previously reported by [76, 77].

Release Kinetics

Table V illustrates a kinetics analysis of the release data, where the vitro release data of PVS from the PVS solution and the optimized NE2 were fitted with the Higuchi model as indicated by the highest value of the coefficient of correlation which indicated diffusion-controlled drug release and the % release of PVS from the F1 patch was best fitted by first order. Korsmeyer- peppas model showed that the diffusional exponent values for the PVS solution and PVS-NE2 were 0.469 and 0.484 respectively indicating a fickian mechanism and 0.51 for the F1 patch which indicates non-fickian mechanism similar results were previously reported [71, 75].

Ex Vivo Skin Permeation Study

The *ex vivo* permeation profile of PVS from the F1 patch is shown in Fig. 4C which demonstrated a gradual rise in the concentration of PVS within 72 h. F1 achieved a maximum amount of (271.66 ± 19 µg/cm^2) permeated across the stratum corneum (SC) within 72 h, high steady-state flux (2.5 ± 0.6 µg.cm^{-2} h^{-1}) and high permeability coefficient (2.9 × 10^{-3} ± 1.4 cm. h^{-1}). The permeation parameters of PVS across rat skin from the F1 patch revealed that the controlled enhancement in cutaneous delivery was made possible by encapsulating PVS in NE2 and loading it onto

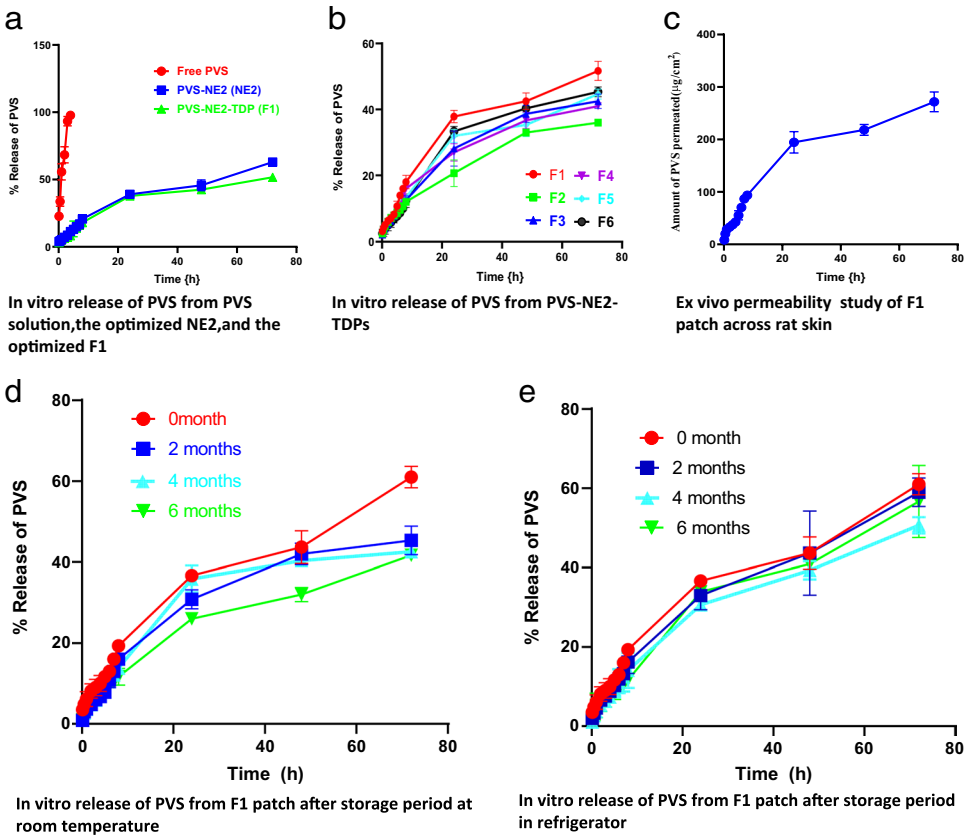

Fig. 4 *In vitro* release profiles of PVS from **a** PVS solution, the optimized NE2 and the optimized F1 **b** PVS-NE2-TDPs **c** *Ex vivo* permeability study of F1 patch across rat skin and **d** *In vitro* release of PVS from F1 patch after storage period at room temperature and **e** *In vitro* release of PVS from F1 patch after storage period in refrigerated temperature (4 ± 2°C)

TDP. Also, the Kinetic analysis of *ex vivo* release data of the optimized F1 was best fitted to the Higuchi model as R^2 values 0.957. In addition, a further examination using the Korsmeyer-peppas model indicated that ($n = 0.598$) non-fickian diffusion mechanism.

The *ex vivo* outcomes can be explained by a variety of methods, such as maintaining close contact between the polymeric matrix of F1 and SC throughout the application and increasing the penetration of PVS across the skin. Besides, the lipophilicity of NEs could improve additional accumulation of PVS in the skin layer and NEs properties including the nano-sized droplets which provide large surface area, the presence of oil, and SC mix act as penetration enhancers [78]. These enhancers can disturb the stratum corneum barrier, enhance fluidization of the lipid matrix, and increase hydration to the stratum corneum [20].

All these factors can occur simultaneously supporting the results found in this study, which showed that the application of NEs as a drug carrier could increase the permeability of hydrophilic drugs [79, 80].

Stability Studies of the Optimized Patch (F1)

At the end of the storage period, there were no changes in the physical appearance of all patches stored in two different temperatures and no significant ($p > 0.05$) change between formulations that had been stored in a refrigerator and those that had been freshly prepared, except for a considerable reduction in % release at 6 months. On the other hand, the formulation that was kept at ambient temperature showed a marked reduction in the % release and drug content as illustrated in Fig. 4D and E. Also, the reduction in % drug release

Table V Kinetic Analysis of PVS Release from PVS Solution and the Optimized NE2 as well as PVS- NE2-TDP (F1)

Formulation code	Correlation coefficient (r^2)			Korsmeyer-Peppas		Main Transport Mechanism
	Zero order	First order	Higuchi model	R^2	n [a]	
PVS solution	0.946	0.908	0.960	0.957	0.469	fickian
NE2	0.935	0.966	0.974	0.913	0.484	Fickian
PVS-NE2-TDP (F1)	0.881	0.973	0.958	0.904	0.51	Non fickian

[a] n is the diffusional exponent of korsmeyer-peppas model

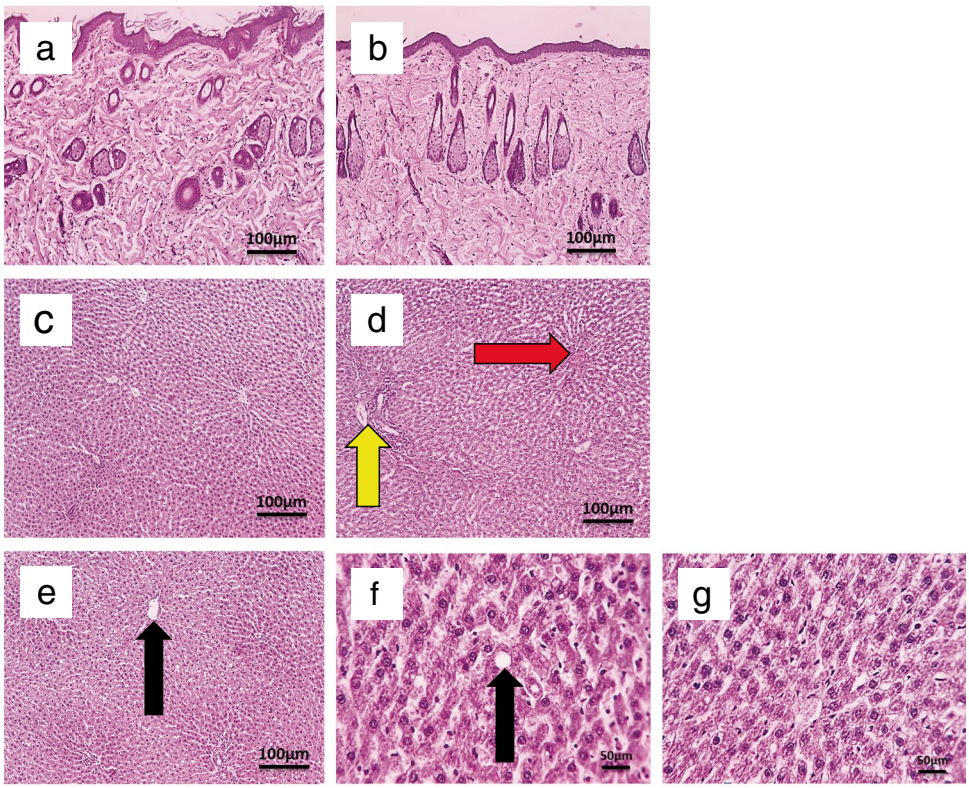

Fig. 5 Microscopic pictures of rat skin **a** untreated **b** treated with the optimized F1 patch. **c** Microscopic images of H&E-stained hepatic sections from **G1** (negative control) demonstrate normal hepatic cord arrangement H surrounding central veins CV with normal portal PA and sinusoids S. **d** Hepatic sections from the **G2** group (positive control) showing larger bile ducts, congested central veins CV (red arrow) and fat vacuoles (yellow arrows) in hepatocytes H. **e** Hepatic sections from **G3** group received oral PVS solution demonstrate mild bile duct dilatation, dilated sinusoids, less mononuclear cell infiltration in portal areas PA, and fewer fat vacuoles in hepatocytes (black arrows) (**c**). **f** Very few fat vacuoles (black arrows), were found in the hepatocytes of the **G4** group (PVS-Patch treated group). **g** Hepatic sections from the **G5** group (**F1 patch**) show partially restored normal organization of hepatic cords H around central veins CV with normal portal areas PA and sinusoids S, hydropic degeneration of periportal hepatocytes

and drug content may be owing to the nature of hydrophilic polymers used in F1 patch preparation [81, 82]. As a result, it is suggested to store patches at lower temperatures similar to findings previously reported [83].

Pharmacodynamics Study of the Optimized Patch (F1)

Skin Irritation Study

After the application of the F1 patch, no erythema or edema was observed in treated or untreated cross-sections of rat skin as shown in Fig. 5a and b. This indicated that the F1 patch was biocompatibility with the skin.

Biomarker Assessment

Effects of the Optimized Patch (F1) on Serum Lipid Profile The pharmacodynamic studies of the optimized F1 patch in comparison with the PVS-oral solution and the PVS-patch were determined using poloxamer 407 induced-hyperlipidemic rats [49] as shown in Table VI. Then, the lipid profiles were evaluated 12 h after poloxamer 407 injection, and it was found that all groups had significantly higher serum levels of TC, TG, HDL, and LDL than the negative control group. In rats, a distinctive feature of poloxamer 407 led to an unusual increase in the levels of HDL [84]. By indirectly stimulating HMG-CoA reductase (a crucial enzyme in the production of cholesterol) the poloxamer 407 (a non-ionic surfactant) can lead to hyperlipidemia in rats [85, 86].

Animals were treated with the F1 patch (G5) for one week, where their serum levels of TC, TG, and HDL significantly improved, and their LDL levels were successfully brought back to normal.

In comparison to the F1 patch, the PVS solution (G3) and PVS-patch (G4) treated groups both could not restore the normal level of LDL in the hyperlipidemic animal model. Figure 6 depicts the serum levels of the examined lipid biomarker after completing the treatment period.

Table VI Effect of Optimized PVS-NE2-TDP (F1), PVS Solution and PVS-TDP on Serum Lipid Profile, Liver Function, Albumin, and Alkaline Phosphatase

Parameter	Time(hr.) / Group	Before treatment	After treatment			
		12 h after induction of hyperlipidemia	3 days	4 days	5 days	1-week
TC (mg/dl)	G1	62.33 ± 4.095 $^{a\,b\,c\,d}$	65 ± 2. $^{a\,b\,c\,d}$	62 ± 7 $^{a\,b\,c\,d}$	66 ± 4. $^{a\,b\,c\,d}$	65 ± 4. $^{a\,b\,c\,d}$
Mean ± SD	G2	449 ± 57*	840 ± 28 $^{*b\,c\,d}$	812 ± 35 $^{*b\,c\,d}$	725 ± 35 $^{*b\,c\,d}$	676 ± 58$^{*b\,c\,d}$
	G3	480 ± 72.2*	435 ± 67.7^{*a}	370 ± 62^{*a}	280 ± 55.8^{*a}	230 ± 48 ^{*a}
	G4	404 ± 36.6*	354.5 ± 67.9^{*a}	305.33 ± 59.5 ^{*a}	269 ± 46 ^{*a}	242 ± 80 ^{*a}
	G5	454.6 ± 84.3*	376.3 ± 73.38 ^{*a}	298 ± 63.4^{*a}	219 ± 46.6^{*a}	164.6 ± 39.2^{*a}
TG (mg/dl)	G1	78 ± 9 $^{a\,b\,c\,d}$	72 ± 7 $^{a\,b\,c\,d}$	77 ± 8 $^{a\,b\,c\,d}$	74 ± 6 $^{a\,b\,c\,d}$	80 ± 6 $^{a\,b\,c\,d}$
Mean ± SD	G2	844 ± 114.17 *	1125 ± 155 $^{*c\,d}$	1130 ± 88 $^{*b\,c\,d}$	941 ± 95$^{*b\,c\,d}$	823 ± 105 $^{*b\,c\,d}$
	G3	877 ± 111*	815 ± 105*	617 ± 60.5 ^{*a}	388 ± 50 ^{*a}	292 ± 424 $^{*a\,d}$
	G4	754 ± 43.2 *	689.66 ± 42.8 *	616.33 ± 65.4 ^{*a}	430.33 ± 84.3 ^{*a}	299 ± 55.6 ^{*a}
	G5	807 ± 121.3*	707.6 ± 120.4*	458.6 ± 95.8 ^{*a}	359 ± 65.7^{*a}	195 ± 41$^{*a\,b}$
HDL (mg/dl)	G1	44 ± 2.5 $^{a\,b\,c\,d}$	48 ± 5 $^{a\,b\,c\,d}$	50 ± 5 $^{a\,b\,c\,d}$	54 ± 8 ^{a}	41 ± 3 ^{a}
Mean ± SD	G2	177 ± 33*	240 ± 44.3^{*c}	305 ± 44^{*c}	280 ± 35 $^{*b\,c}$	302 ± 17 $^{*b\,c\,d}$
	G3	1196 ± 58*	1189 ± 18*	160 ± 60 *	131 ± 55 ^{a}	85 ± 33.4 ^{a}
	G4	133 ± 16*	98 ± 8^{*a}	94.6 ± 37.8 ^{*a}	96 ± 28.5 ^{a}	92 ± 23 ^{a}
	G5	192 ± 59.7*	183.3 ± 32*	148 ± 40.4*	96 ± 30 ^{a}	77 ± 28 ^{a}
LDL (mg/dl)	G1	4 ± 1.1 $^{a\,b\,c\,d}$	6 ± 1.155 $^{a\,b\,c\,d}$	6 ± 1.155 $^{a\,b\,c\,d}$	6 ± 0.8 $^{a\,b\,c\,d}$	10.2 ± 1 $^{a\,b\,c}$
Mean ± SD	G2	108 ± 4.9*	386 ± 79 $^{*b\,c\,d}$	289 ± 21 $^{*b\,c\,d}$	270 ± 16.8 $^{*b\,c}$	208 ± 27 $^{*b\,c\,d}$
	G3	111.66 ± 7.3 *	82.666 ± 34 ^{*a}	79.66 ± 1.76 ^{*a}	80 ± 4 $^{*a\,d}$	80 ± 5 ^{*a}
	G4	120 ± 15 *	109.33 ± 50.6 ^{*a}	87 ± 10.5^{*a}	87.3 ± 1.3 $^{*a\,d}$	90.6 ± 8.5 $^{*a\,d}$
	G5	101.5 ± 5*	51.33 ± 21 ^{*a}	57 ± 4.2^{*a}	51 ± 3.6$^{*b\,c}$	43 ± 12 $^{a\,b}$
ALT(U/L)	G1	-	-	-	-	27.7 ± 3.2 ^{abc}
	G2					62 ± 6.3 ^{*d}
	G3					44 ± 3*
	G4					48 ± 1.15^{*d}
	G5					36.7 ± 2.02 ^{ac}
AST(U/L)	G1	-	-	-	-	94.6 ± 4.1 ^{abc}
	G2					223 ± 15.5$^{*b\,c\,d}$
	G3					152 ± 5 $^{*a\,d}$
	G4					125 ± 6.8^{*a}
	G5					104.66 ± 6.7$^{a\,b}$
ALP(U/L)	G1	-	-	-	-	257 ± 10 $^{a\,b\,c\,d}$
	G2					407 ± 11.6 ^{*d}
	G3					369.5 ± 18.6 ^{*d}
	G4					376 ± 13.8^{*d}
	G5					299.7 ± 3.2 ^{abc}
Albumin(gm/dl)	G1	-	-	-	-	4.9 ± 0.13 ^{abc}
	G2					3.4 ± 0.18 $^{*b\,d}$
	G3					4 ± 0.05 $^{*a\,c}$
	G4					3.85 ± 0.068$^{*b\,d}$
	G5					4.34 ± 0.08 ^{ac}

G1: Normal control

G2: Non treated hyperlipidemic rats (Positive control)

G3: Orally treated hyperlipidemic rats with PVS solution

G4: transdermally treated hyperlipidemic rat by PVS-TDP

G5 transdermally treated hyperlipidemic rat by PVS-NE2-TDP (F1)

TC, total cholesterol; TG, triglycerides; HDL, high density lipoprotein; LDL, low-density lipoprotein

Values are presented as mean ± SEM. (n = 6)

* Denotes significantly different from the value of negative control;

^{a} Denotes significantly different from the value of positive control

^{b} Denotes significantly different from the value of PVS solution

^{c} Denotes significantly different from PVS-TDP

^{d} Denotes significantly different from PVS-NE2-TDP

The statistical analysis was conducted using Students' *t*-test (unpaired) at $p < 0.05$

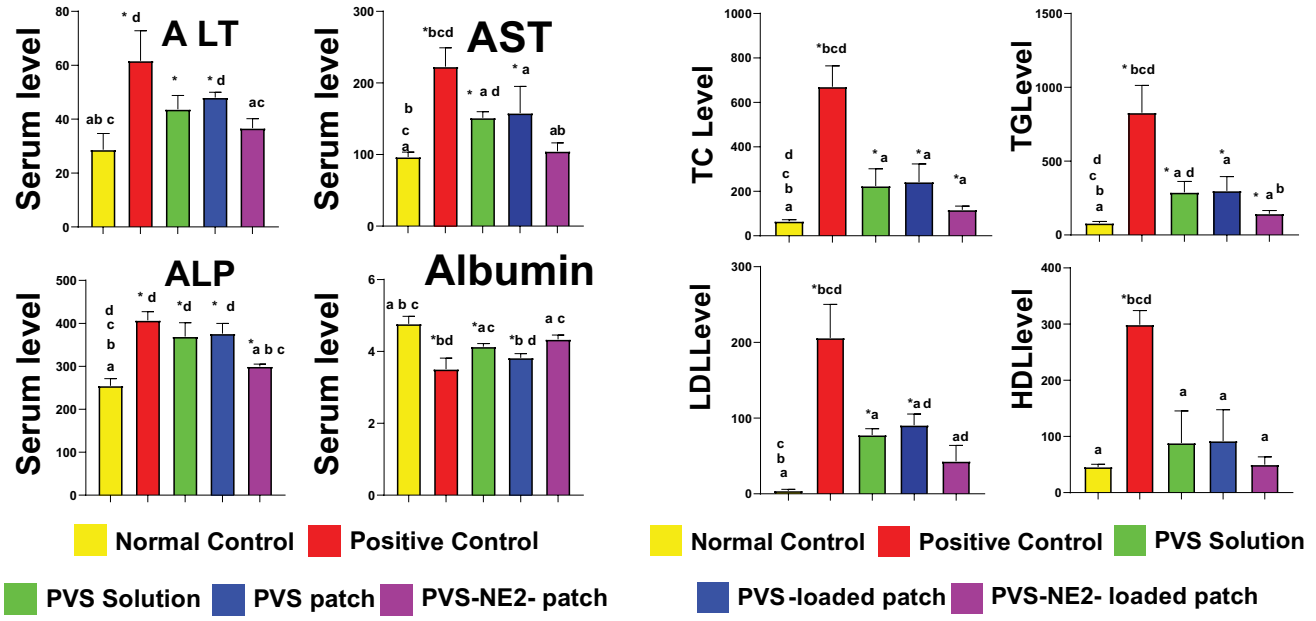

Fig. 6 The serum level of the tested lipid biomarker and the liver function following the completion of the treatment period with PVS solution, PVS- patch and PVS-NE2-Patch (F1) (10 mg/Kg) are showed in Fig. 6. **Notes:** values were presented as means ± SEM ($n = 6$ rats); *: denotes significantly different from the value of **G1** (negative control); **a**: denotes significantly different from the value of **G2** (positive control); **b**: denotes significantly different from the value of **G3** (PVS) solution; **c**: denotes significantly different from the value of **G4** (PVS-TDP) and **d**: denotes significantly different from the value of **G5** (PVS-NE2-TDP). At $p < 0.05$, the statistical analysis was carried out using Student's *t*-test (unpaired). **Abbreviations:** (ALT) Alanine aminotransferases, (ALT) aspartate aminotransferases, (ALP) alkaline phosphatase, (TC) total cholesterol, (TG) triglycerids, (LDL) low-density lipoprotein, (HDL) high density lipoprotein

Considering the study outcome, PVS-NE2-TDP (F1) showed a promising effect on lipid levels this could be due to the action of NEs in improving the transdermal permeation because of their smaller droplets as well as higher lipophilicity that enhances PVS permeability [87, 88].

Effects of the Optimized Patch (F1) on Liver Functions A clear elevation in the liver enzymes (Alanine aminotransferases (ALT), Aspartate aminotransferases (ALT), and Alkaline Phosphatase (ALP) in rats injected with poloxamer 407. This may be because hyperlipidemia has been considered a common risk factor for liver diseases as high fat levels increase liver oxidative stress [89]. Treatment with PVS solution and PVS-patch caused liver enzymes to significantly decrease, and the albumin level to slightly increase without returning to the normal level. However, treatment with the optimized patch (F1) significantly improved liver function, reduced liver serum enzymes, and raised the albumin levels and restored their levels to normal as shown in Table VI and Fig. 6. The results indicated that the F1 patch might be used as a PVS drug delivery system. The controlled transdermal delivery of PVS is improved by encapsulating the drug in NE2 and loading it into a patch [90].

Histopathological Examination In the current study, histopathological analysis supported the biochemical findings. Light microscopic examination of liver sections from the G1 group revealed the central vein (CV) and surrounding hepatocytes to have a normal histological structure (Fig. 5C). Liver sections of G2 displayed a diffuse fatty change surrounding the hepatocytes, dilated bile ducts, a clogged CV, a few inflammatory cells, and dilated sinusoids (Fig. 5D). Liver tissues of the G3 group displayed mild bile duct dilation, mild portal congestion, dilated sinusoids, and fewer fat vacuoles in hepatocytes (Fig. 5E). Liver tissues from G4 show a slightly dilated sinusoids S and small number of fat vacuoles in hepatocytes (Fig. 5F). Liver sections from G5 exhibit normal sinusoids S and portal areas PA, periportal hepatocyte hydropic degeneration, a partially restored normal organization of hepatic cords H around central veins CV (Fig. 5G) [91].

The G1 group's quadriceps muscles microscopic examination revealed that both the longitudinal and crossed sections of the bundles have a normal histological structure (Fig. 7-A1, A2) respectively. The G2 group displayed mild mononuclear cell infiltration, atrophied myocytes, and hyaline degeneration in some sections (Fig. 7B1, B2). The G3 group (Fig. 7C1, C2) exhibits a moderate level of lipid infiltration in the muscle fibers. In comparison to somewhat higher levels of lipid infiltration in the muscle fibers in the G4 group (control patch) (Fig. 7-D1, D2) and lower levels in the G5 group (received F1 patch) (Fig. 7-E1, E2), we

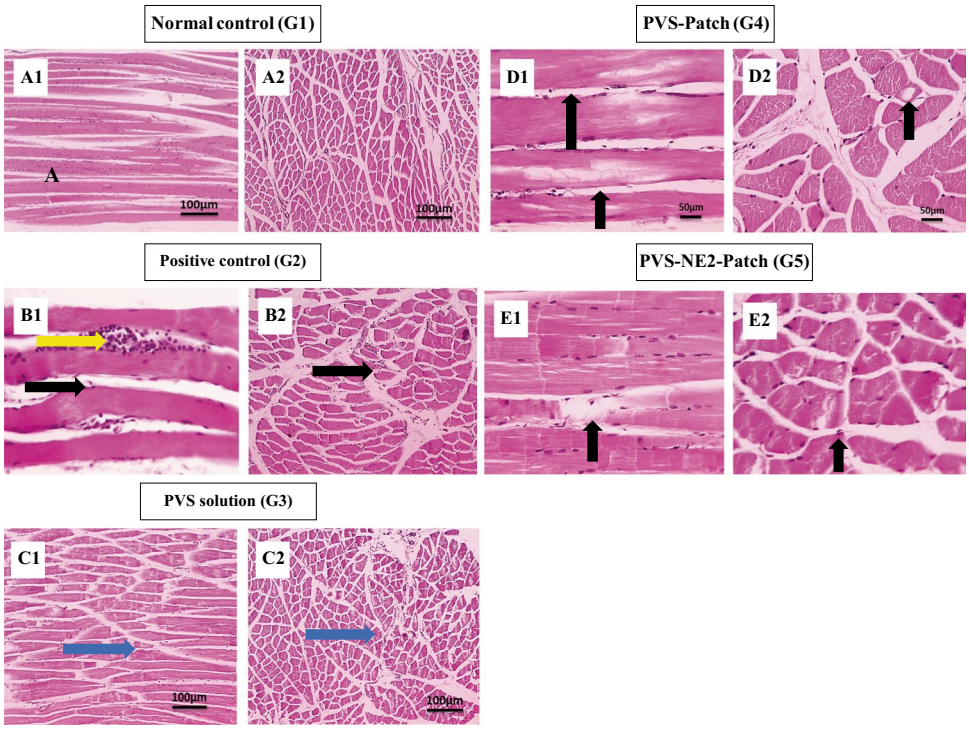

Fig. 7 Microscopic images of longitudinally sectioned skeletal muscles stained with H&E reveal a normal arrangement of striated muscle fibers with nuclei in the periphery in the **G1** group **(A1).** The longitudinally sectioned skeletal muscles from the **G2** group (**B1**) demonstrate substantial lipid infiltration and hyaline degeneration (black and yellow arrows) in several areas. The skeletal muscles in the **G3** group (received oral PVS solution) (**C1**) had moderate lipid infiltration in the muscle fibers (blue arrows). The **G4** group (received control patch) **(D1)** showed higher lipid levels in muscle fiber compared to the **G5** group (received F1 patch) **(E1).** Microscopic images of H&E-stained cross-sectioned skeletal muscles show healthy muscle fibers with nuclei that are positioned peripherally in the **G1** group **(A2).** The cross-sectioned skeletal muscles from the **G2** group **(B2**) exhibit mild mononuclear cell infiltration**,** hyaline degeneration, and slightly higher lipid infiltration in muscle fibers. (black arrow) **G3** group **(C2)** had moderate lipid infiltration in the muscle fibers (blue arrows). **G4** had slightly higher lipid infiltration in the muscle fibers (black arrows). The **G5** group treated with **F1 patch (E2)** had very mild lipid infiltration in the muscle fibers (black arrows)

concluded that PVS-NE2-TDP (F1 patch) could be considered a promising nanocarrier system for transdermal delivery of PVS by passing drug degradation that occurs in oral routs similar findings were declared previously [88].

Conclusion

PVS-NEs were successfully prepared by aqueous phase titration method using 50%v/v oleic acid as the continuous phase, 40% v/v SC mix, and 10% v/v deionized water as the dispersed phase. PVS-NE2 was selected as an optimum formula as it showed the smallest PS (251 ± 16) nm with narrow size distribution PDI (0.4 ± 0.16), the highest ZP (-70 ± 10.4) mv, and the highest drug content (100 ± 3.8) %. So NE2 was selected for further evaluation to be incorporated into TDPs. PVS-NE2-TDPs (F1) were prepared using solvent evaporation method. FT-IR navigates interaction between PVS and other oils or polymers used in F1 preparation. TEM image of NE2 showed that NE2 droplets were dark, spherical in shape, and well dispersed. The PVS released from the prepared formulations could be arranged as follows: F1 > F3 > F6 > F5 > F4 > F2. So, F1 was selected as an optimum patch as it showed satisfactory physicochemical properties and a higher % release of PVS compared to other patches of different polymers. *Ex vivo* permeation studies of F1 showed that the formulation was dermatologically safe and almost total skin permeation of PVS 271.66 ± 19 µg/cm^2 in 72 h. The *in vivo* study demonstrated that PVS-NE-TDP (F1) was more effective at lowering lipid levels as evidenced by blood analysis and histopathological examination. Finally, our results prove that PVS-NE2-TDP can be a good treatment for hyperlipidemia with higher efficacy by passing the first-pass effect.

Supplementary Information The online version contains supplementary material available at https://doi.org/10.1208/s12249-024-02746-5.

Acknowledgements The authors are particularly grateful for the assistance given by Dr. Noha El-Wassefy, Professor, Department of Biometrics, Faculty of Dentistry, Mansoura University, for her assistance in measuring the tensile strength of patches. The authors would also like

to express their gratitude to Dr Walaa Awadin, Professor, Department of Pathology, Faculty of Veterinary Medicine, Mansoura University, for her technical support and specimen examination during the histopathological examination.

Author Contribution Each author contributed to the planning and design of the study. Data collection, material preparation, and analysis were carried out by Seham I Elsayed, Marwa S El- Dahan, and Germeen N S Girgis. The manuscript's initial draft was written by Seham I Elsayed, and all other writers offered their feedback on earlier drafts. The final manuscript was reviewed and approved by all authors.

Funding Open access funding provided by The Science, Technology & Innovation Funding Authority (STDF) in cooperation with The Egyptian Knowledge Bank (EKB). The assistance of Mansoura University for this research is gratefully acknowledged by the authors.

Data Availability On request, raw data and materials are accessible from the corresponding author.

Declarations

Ethical Approval All institutional and national guidelines for the care and usage of laboratory animals were followed.

Consent for Publication The submission of this research paper to AAPS Pharm Sci Tech has the approval of all authors.

Competing Interests The authors declare they have no competing interests.

References

1. Korani S, Korani M, Bahrami S, Johnston TP, Butler AE, Banach M, et al. Application of nanotechnology to improve the therapeutic benefits of statins. Drug Discov Today. 2019;24(2):567–74.
2. Holvoet P, Jenny NS, Schreiner PJ, Tracy RP, Jacobs DR. The relationship between oxidized LDL and other cardiovascular risk factors and subclinical CVD in different ethnic groups: the Multi-Ethnic Study of Atherosclerosis (MESA). Atherosclerosis. 2007;194(1):245–52.
3. Verma N. Introduction to hyperlipidemia and its treatment: a review. Int J Curr Pharm Res. 2016;9:6–14.
4. Singhvi SM, Pan HY, Morrison RA, Willard DA. Disposition of pravastatin sodium, a tissue-selective HMG-CoA reductase inhibitor, in healthy subjects. Br J Clin Pharmacol. 1990;29(2):239–43.
5. Saraogi GK, Tholiya S, Mishra Y, Mishra V, Albutti A, Nayak P, et al. Formulation development and evaluation of pravastatin-loaded nanogel for hyperlipidemia management. Gels. 2022;8(2):81.
6. Kawata S, Yamasaki E, Nagase T, Inui Y, Ito N, Matsuda Y, et al. Effect of pravastatin on survival in patients with advanced hepatocellular carcinoma. A randomized controlled trial. Br J Cancer. 2001;84(7):886–91.
7. Graf H, Jüngst C, Straub G, Dogan S, Hoffmann RT, Jakobs T, et al. Chemoembolization combined with pravastatin improves survival in patients with hepatocellular carcinoma. Digestion. 2008;78(1):34–8.
8. Rizg WY, Hosny KM, Eshmawi BA, Alamoudi AJ, Safhi AY, Murshid SSA, et al. Tailoring of geranium oil-based nanoemulsion loaded with pravastatin as a nanoplatform for wound healing. Polymers (Basel). 2022;14(9):1912.
9. Tayel SA, El-Nabarawi MA, Tadros MI, Abd-Elsalam WH. Duodenum-triggered delivery of pravastatin sodium: II. Design, appraisal and pharmacokinetic assessments of enteric surface-decorated nanocubosomal dispersions. Drug Deliv. 2016;23(9):3266–78.
10. Gurpreet K, Singh S. Review of nanoemulsion formulation and characterization techniques. Indian J Pharm Sci. 2018;80(5):781–9.
11. Ghosh V, Mukherjee A, Chandrasekaran N. Ultrasonic emulsification of food-grade nanoemulsion formulation and evaluation of its bactericidal activity. Ultrason Sonochem. 2013;20(1):338–44.
12. Rashidi L, Khosravi-Darani K. The applications of nanotechnology in food industry. Crit Rev Food Sci Nutr. 2011;51(8):723–30.
13. Sithole MN, Marais S, Maree SM, Du Plessis LH, Du Plessis J, Gerber M. Development and characterization of nano-emulsions and nano-emulgels for transdermal delivery of statins. Expert Opin Drug Deliv. 2021;18(6):789–801.
14. Badran MM, Harisa GI, AlQahtani SA, Alanazi FK, Zoheir KMA. Pravastatin-loaded chitosan nanoparticles: Formulation, characterization and cytotoxicity studies. J Drug Deliv Sci Technol. 2016;32:1–9.
15. Jaiswal M, Dudhe R, Sharma PK. Nanoemulsion: an advanced mode of drug delivery system. 3 Biotech. 2015;5(2):123–7.
16. Abd E, Benson HA, Roberts MS, Grice JE. Minoxidil skin delivery from nanoemulsion formulations containing eucalyptol or oleic acid: Enhanced diffusivity and follicular targeting. Pharmaceutics. 2018;10(1):19.
17. Shaker DS, Ishak RA, Ghoneim A, Elhuoni MA. Nanoemulsion: A review on mechanisms for the transdermal delivery of hydrophobic and hydrophilic drugs. Sci Pharm. 2019;87(3):17.
18. Nogoy KMC, Kim HJ, Lee Y, Zhang Y, Yu J, Lee DH, et al. High dietary oleic acid in olive oil-supplemented diet enhanced omega-3 fatty acid in blood plasma of rats. Food Sci Nutr. 2020;8(7):3617–25.
19. Kogan A, Garti N. Microemulsions as transdermal drug delivery vehicles. Adv Colloid Interface Sci. 2006;123–126:369–85.
20. Alkilani AZ, McCrudden MT, Donnelly RF. Transdermal Drug Delivery: Innovative pharmaceutical developments based on disruption of the barrier properties of the stratum corneum. Pharmaceutics. 2015;7(4):438–70.
21. Priya S, Koland M, Kumari S. Nanoemulsion components screening of quetiapine fumarate: Effect of surfactant and co surfactant. Asian J Pharm Clin Res. 2015;8:136–40.
22. Wu H, Ramachandran C, Weiner ND, Roessler BJ. Topical transport of hydrophilic compounds using water-in-oil nanoemulsions. Int Pharm. 2001;220(1):63–75.
23. Ramadan E, Borg T, Abdelghani GM, Saleh N. Formulation and evaluation of acyclovir microemulsions. Bull Pharm Sci. 2013;36:31–47.
24. Jain K, Kumar R, Sood S, Kuppusamy G. Enhanced oral bioavailability of atorvastatin via oil-in-water nanoemulsion using aqueous titration method. JPSR. 2013;5:18–25.
25. Niknam SM, Kashaninejad M, Escudero I, Sanz MT, Beltrán S, Benito JM. Preparation of water-in-Oil nanoemulsions ioaded with phenolic-rich olive cake extract using response surface methodology approach. Foods. 2022;11(3):279.

26. Kaur R, Ajitha M. Formulation of transdermal nanoemulsion gel drug delivery system of lovastatin and its in vivo characterization in glucocorticoid induced osteoporosis rat model. JDDST. 2019;52:968–78.
27. Polychniatou V, Tzia C. Study of formulation and stability of cosurfactant free water-in-olive oil nano- and submicron emulsions with food grade non-ionic surfactants. JAOCS. 2014;91:79–88.
28. Almajidi Y, Mahdi Z, Maraie N. Preparation and in vitro evaluation of montelukast sodium oral nanoemulsion. Int App Pharm. 2018;10:49.
29. Rajitha P, Shammika P, Aiswarya S, Gopikrishnan A, Jayakumar R, Sabitha M. Chaulmoogra oil based methotrexate loaded topical nanoemulsion for the treatment of psoriasis. JDDST. 2019;49:463–76.
30. Ali MS, Alam MS, Alam N, Siddiqui MR. Preparation, characterization and stability study of dutasteride loaded nanoemulsion for treatment of benign prostatic hypertrophy. Iran J Pharm Res. 2014;13(4):1125–40.
31. Shehata TM, Mohafez O, Hanieh HN. Pharmaceutical formulation and biochemical evaluation of atorvastatin transdermal patches. Indian J Pharm Educ Res. 2018;52:54–61.
32. Ahmed TA, Bawazir AO, Alharbi WS, Safo MK. Enhancement of simvastatin ex vivo permeation from mucoadhesive buccal films ioaded with dual drug release carriers. Int J Nanomedicine. 2020;15:4001–20.
33. Anter HM, Abu Hashim II, Awadin W, Meshali MM. Novel anti-inflammatory film as a delivery system for the external medication with bioactive phytochemical "Apocynin." Drug Des Devel Ther. 2018;12:2981–3001.
34. Allam A, Fetih G. Sublingual fast dissolving niosomal films for enhanced bioavailability and prolonged effect of metoprolol tartrate. Drug Des Devel Ther. 2016;10:2421–33.
35. Singh A, Bali A. Formulation and characterization of transdermal patches for controlled delivery of duloxetine hydrochloride. JAST. 2016;7(1):25.
36. David SR, Malek N, Mahadi AH, Chakravarthi S, Rajabalaya R. Development of controlled release silicone adhesive-based mupirocin patch demonstrates antibacterial activity on live rat skin against Staphylococcus aureus. Drug Des Devel Ther. 2018;12:481–94.
37. Suksaeree J, Monton C, Madaka F, Chusut T, Saingam W, Pichayakorn W, et al. Formulation, physicochemical characterization, and in vitro study of chitosan/HPMC blends-based herbal blended patches. AAPS PharmSciTech. 2015;16(1):171–81.
38. Zaid Alkilani A, Hamed R, Al-Marabeh S, Kamal A, Abu-Huwaij R, Hamad I. Nanoemulsion-based film formulation for transdermal delivery of carvedilol. JDDST. 2018;46:122–8.
39. Parhi R, Suresh P. Transdermal delivery of diltiazem HCl from matrix film: Effect of penetration enhancers and study of antihypertensive activity in rabbit model. J Adv Res. 2016;7(3):539–50.
40. Ramadan E, Borg T, Abdelghani G, Saleh NM. Transdermal microneedle-mediated delivery of polymeric lamivudine-loaded nanoparticles. J Pharm Technol Drug Res. 2016;5(1):1.
41. Dash S, Murthy PN, Nath L, Chowdhury P. Kinetic modeling on drug release from controlled drug delivery systems. Acta Pol Pharm. 2010;67(3):217–23.
42. Costa P, Lobo JMS. Modeling and comparison of dissolution profiles. Eur J Pharm Sci. 2001;13(2):123–33.
43. Higuchi T. Rate of Release of Medicaments from ointment bases containing drugs in suspension. J Pharm Sci. 1961;50(10):874–5.
44. Korsmeyer R, Gurny R, Doelker E, Buri P, Peppas N. Mechanisms of potassium chloride release from compressed, hydrophilic, polymeric matrices: effect of entrapped air. J Pharm Sci. 1983;72(10):1189–91.
45. Panchagnula R, Bokalial R, Sharma P, Khandavilli S. Transdermal delivery of naloxone: skin permeation, pharmacokinetic, irritancy and stability studies. Int J Pharm. 2005;293(1–2):213–23.
46. Dalaklioglu S, Sahin P, Tasatargil A, Celik-Ozenci C. Pravastatin improves the impaired nitric oxide-mediated neurogenic and endothelium-dependent relaxation of corpus cavernosum in aged rats. Aging Male. 2014;17(4):259–66.
47. Al Hanbali OA, Khan HMS, Sarfraz M, Arafat M, Ijaz S, Hameed A. Transdermal patches: Design and current approaches to painless drug delivery. Acta Pharm. 2019;69(2):197–215.
48. Elsayed SI, Girgis GNS, El-Dahan MS. Formulation and evaluation of pravastatin sodium-ioaded PLGA nanoparticles: In vitro–in vivo studies assessment. Int J Nanomedicine. 2023;18:721–42.
49. Fathi HA, Allam A, Elsabahy M, Fetih G, El-Badry M. Nanostructured lipid carriers for improved oral delivery and prolonged antihyperlipidemic effect of simvastatin. Colloids Surf B Biointerfaces. 2018;162:236–45.
50. Rizvi SZH, Shah FA, Khan N, Muhammad I, Ali KH, Ansari MM, et al. Simvastatin-loaded solid lipid nanoparticles for enhanced anti-hyperlipidemic activity in hyperlipidemia animal model. Int J Pharm. 2019;560:136–43.
51. Cocchetto DM, Bjornsson TD. Methods for vascular access and collection of body fluids from the laboratory rat. J Pharm Sci. 1983;72(5):465–92.
52. Abo-zalam HB, El-Denshary ES, Abdelsalam RM, Khalil IA, Khattab MM, Hamzawy MA. Therapeutic advancement of simvastatin-loaded solid lipid nanoparticles (SV-SLNs) in treatment of hyperlipidemia and attenuating hepatotoxicity, myopathy and apoptosis: Comprehensive study. Biomed Pharmacother. 2021;139: 111494.
53. Harrison C. Carleton. BMJ. 1967;4(5570):46.
54. Bancroft JD, Gamble M. Theory and practice of histological techniques. Elsevier health sciences; 2008. p.105–21.
55. Azmi NAN, Elgharbawy AAM, Motlagh SR, Samsudin N, Salleh HM. Nanoemulsions: Factory for food, pharmaceutical and cosmetics. Processes. 2019;7:617.
56. Sarheed O, Dibi M, Ramesh K. Studies on the effect of oil and surfactant on the formation of alginate-based o/w Lidocaine nanocarriers using nanoemulsion template. Pharmaceutics. 2020;12(12):1223.
57. Baba Shekh AO, Abdul Wahab R, Yahya NA. Formulation of roselle extract water-in-oil nanoemulsion for controlled pulmonary delivery. J Dispers Sci Technol. 2023;44(10):1830–41.
58. Shukla A, Janich M, Jahn K, Krause A, Kiselev MA, Neubert RH. Investigation of pharmaceutical oil/water microemulsions by small-angle scattering. Pharm Res. 2002;19(6):881–6.
59. Aithal G, Nayak U, Mehta C, Narayan R, Gopalkrishna P, Pandiyan S, et al. Localized in situ nanoemulgel drug delivery system of quercetin for periodontitis: Development and computational simulations. Molecules. 2018;23:1363.
60. Su R, Yang L, Wang Y, Yu S, Guo Y, Deng J, et al. Formulation, development, and optimization of a novel octyldodecanol-based nanoemulsion for transdermal delivery of ceramide IIIB. Int J Nanomedicine. 2017;12:5203–21.
61. Yulianita R, Sopyan I, Muchtaridi M. Forced degradation study of statins: a review. Int J App Pharm. 2018;10:38.
62. Sarheed O, Shouqair D, Ramesh K, Khaleel T, Amin M, Boateng J, et al. Formation of stable nanoemulsions by ultrasound-assisted two-step emulsification process for topical drug delivery: Effect of oil phase composition and surfactant concentration and loratadine as ripening inhibitor. Int J Pharm. 2020;576: 118952.
63. Rao J, McClements DJ. Stabilization of Phase inversion temperature nanoemulsions by surfactant displacement. J Agric Food Chem. 2010;58(11):7059–66.
64. Mehanna MM, Shabarek MI, Elmaradny HA, Elmartadny HA. Spray-dried pH-sensitive microparticles: effectual methodology to ameliorate the bioavailability of acid labile pravastatin. Drug Dev Ind Pharm. 2019;45(3):485–97.
65. Al-Badr AA, Mostafa GA. Pravastatin sodium. Profiles Drug Subst Excip Relat Methodol. 2014;39:433–513.

66. Liang J, Li H, Yan J, Hou W. Demulsification of oleic-acid-coated magnetite nanoparticles for cyclohexane-in-water nanoemulsions. Energy Fuels. 2014;28(9):6172–8.
67. Fu X, Weibo K, Zhang Y, Jiang L, Wang J, Lei J. Novel solid-solid phase change materials with biodegradable trihydroxy surfactant for thermal energy storage. RSC Adv. 2015;5:68881–9.
68. Khanum H, Ullah K, Murtaza G, Khan SA. Fabrication and in vitro characterization of HPMC-g-poly (AMPS) hydrogels loaded with loxoprofen sodium. Int J Biol Macromol. 2018;120:1624–31.
69. Taher MA, Lo'ay AA, Gouda M, Limam SA, Abdelkader MFM, Osman SO, et al. Impacts of gum arabic and polyvinylpyrrolidone (PVP) with salicylic acid on peach fruit (Prunus persica) shelf life. Molecules. 2022;27(8):2595.
70. Sharma A, Jain C. Preparation and characterization of solid dispersions of carvedilol with PVP K30. Res Pharm Sci. 2010;5(1):49.
71. Shivalingam M, Balasubramanian A, Ramalingam K. Formulation and evalution of transdermal patches of pantoprazole sodium. Int J App Pharm. 2021;31(5):287–91.
72. Ahmad N, Ahmad R, Mohammed Buheazaha T, Salman AlHomoud H, Al-Nasif HA, Sarafroz M. A comparative ex vivo permeation evaluation of a novel 5-fluorocuracil nanoemulsion-gel by topically applied in the different excised rat, goat, and cow skin. Saudi J Biol Sci. 2020;27(4):1024–40.
73. Agnihotri N, Soni GC, Prajapati SK, Chanchal DK, Khan A, Tiwari S, editors. Formulation and evaluation of nanoemulsion for targeting and systemic delivery of diclofenac sodium. Sch Acad J Pharm. 2019;8(8):376–93.
74. Xiao Y, Zhang WL, Liu JP, Lin ZY, Wang L, Yu PP. Preparation and in vitro characterization of a transdermal patch containing nisoldipine. J Int Pharm Res 2013;40:365–8.
75. Latif MS, Al-Harbi FF, Nawaz A, Rashid SA, Farid A, Mohaini MA, et al. Formulation and evaluation of hydrophilic polymer based methotrexate patches: In vitro and in vivo characterization. Polymers (Basel). 2022;14(7):1310.
76. Kumar M, Trivedi VR, Shukla AK, Dev SK. Effect of polymers on the physicochemical and drug release properties of transdermal patches of atenolol. Int J App Pharm. 2018;10(4):68–73.
77. Sadhasivam L, Dey N, Francis AP, Devasena T. Transdermal patches of chitosan nanoparticles for insulin delivery. Int J Pharm Pharm Sci. 2015;7:84–8.
78. Hamed R, Basil M, AlBaraghthi T, Sunoqrot S, Tarawneh O. Nanoemulsion-based gel formulation of diclofenac diethylamine: design, optimization, rheological behavior and in vitro diffusion studies. Pharm Dev Technol. 2016;21(8):980–9.
79. Gul U, Khan MI, Madni A, Sohail MF, Rehman M, Rasul A, et al. Olive oil and clove oil-based nanoemulsion for topical delivery of terbinafine hydrochloride: in vitro and ex vivo evaluation. Drug Deliv. 2022;29(1):600–12.
80. Zaid Alkilani A, Hamed R, Hussein G, Alnadi SH. Nanoemulsion-based patch for the dermal delivery of ascorbic acid. J Dispers Sci Technol. 2021;43:1–11.
81. Prabhakara P, Koland M, Vijaynarayana K, Harish NM, Shankar G, Ahmed MG, Narayana C, Satyanarayana D. Preparation and evaluation of transdermal patches of papaverine hydrochloride. Int J Res Pharm Sci. 2010;1(3):259–26.
82. Kusum Devi V, Saisivam S, Maria GR, Deepti PU. Design and evaluation of matrix diffusion controlled transdermal patches of verapamil hydrochloride. Drug Dev Ind Pharm. 2003;29(5):495–503.
83. Hashmat D, Shoaib MH, Ali FR, Siddiqui F. Lornoxicam controlled release transdermal gel patch: Design, characterization and optimization using co-solvents as penetration enhancers. PLoS ONE. 2020;15(2): e0228908.
84. Ahmed T. Study the pharmacokinetics, pharmacodynamics and hepatoprotective activity of rosuvastatin from drug loaded lyophilized orodispersible tablets containing transfersomes nanoparticles. JDDST. 2021;63: 102489.
85. Harvey RA, Clark M, Finkel R, Rey J, Whalen K. Lippincott's illustrated reviews: Pharmacology. Philadelphia; 2012. p.413–25
86. Castañeda PS, Escobar-Chávez JJ, Vázquez JA, Cruz IMR, Contreras LMM. Pravastatin transdermal patches: Effect of the formulation and two different lengths of microneedles on in-vitro percutaneous absorption studies. Iran J Pharm Res. 2020;19(2):127–33.
87. Kakadia PG, Conway BR. Design and development of essential oil based nanoemulsion for topical application of triclosan for effective skin antisepsis. Pharm Dev Technol. 2022;27(5):554–64.
88. Mahmoud MO, Aboud HM, Hassan AH, Ali AA, Johnston TP. Transdermal delivery of atorvastatin calcium from novel nanovesicular systems using polyethylene glycol fatty acid esters: Ameliorated effect without liver toxicity in poloxamer 407-induced hyperlipidemic rats. J Control Release. 2017;254:10–22.
89. Dangl M, Eisenberg T, Grant JK, Vincent L, Colombo R, Sancassani R, et al. A comprehensive review of coronary artery disease in patients with end-stage liver disease. Transplant Rev (Orlando). 2022;36(3): 100709.
90. Eltellawy YA, El-Kayal M, Abdel-Rahman RF, Salah S, Shaker DS. Optimization of transdermal atorvastatin calcium – Loaded proniosomes: Restoring lipid profile and alleviating hepatotoxicity in poloxamer 407-induced hyperlipidemia. Int J Pharm. 2021;593: 120163.
91. Kassem AM, Ibrahim HM, Samy AM. Development and optimisation of atorvastatin calcium loaded self-nanoemulsifying drug delivery system (SNEDDS) for enhancing oral bioavailability: in vitro and in vivo evaluation. J Microencapsul. 2017;34(3):319–33.